Appl. Magn. Reson. 22, 421–430 (2002)

Applied Magnetic Resonance

The Mo-OH Proton of the Low-pH Form of Sulfite Oxidase: Comparison of the Hyperfine Interactions Obtained from Pulsed ENDOR, CW-EPR and ESEEM Measurements

A. V. Astashkin[1,*], A. M. Raitsimring[1], C. Feng[1], J. L. Johnson[2] K. V. Rajagopalan[2], and J. H. Enemark[1]

[1] Department of Chemistry, University of Arizona, Tucson, Arizona, USA
[2] Department of Biochemistry, Duke University Medical Center, Durham, North Carolina, USA

Received March 22, 2002; revised April 3, 2002

Abstract. Pulsed electron nuclear double resonance (ENDOR) spectra have been obtained for the exchangeable Mo-OH proton of the low-pH form of native chicken liver sulfite oxidase (SO) and recombinant human SO for the first time. The spectra of the two enzymes are very similar, indicating a similar binding geometry of the hydroxyl ligand to the Mo center. The isotropic hyperfine interaction (hfi) constant for the proton of the OH ligand in both enzymes is about 26 MHz. The anisotropic components of the hfi obtained from the pulsed ENDOR spectra are about 1.6–1.8 times larger than those obtained by continuous-wave electron paramagnetic resonance and electron spin echo envelope modulation. These hfi differences are explained by a rotational disorder of the Mo-OH group. A similar rotational disorder of the coordinated exchangeable ligand has been found previously for the high-pH and phosphate-inhibited forms of SO.

1 Introduction

Sulfite oxidase (SO) is a physiologically vital enzyme that catalyzes the oxidation of sulfite to sulfate, the final step in sulfur metabolism in vertebrates. The crystal structure of oxidized SO shows a five-coordinated distorted square pyramidal molybdenum center with a terminal oxo group in the apical position and thiolate S atoms in three of the equatorial positions. The fourth equatorial position is occupied by an O atom that appears to be an OH- or H_2O ligand on the basis of the long Mo-O bond distance [1]. However, studies on polycrystalline oxidized SO by X-ray absorption spectroscopy show a Mo(VI) center with two

* On leave from the Institute of Chemical Kinetics and Combustion, Russian Academy of Sciences, Novosibirsk, Russian Federation

terminal oxo groups [2]. These combined results suggest that during the X-ray crystal structure determination the Mo center of SO may have become reduced to Mo(V) or Mo(IV) in the intense synchrotron radiation beam. The proposed mechanism for SO involves a transfer of the equatorial oxygen atom, followed by successive coupled electron/proton transfers, with Mo passing through the Mo(V) oxidation state [3–5]. Thus, the number of exchangeable protons on the equatorial oxygen atom plays a central role in understanding the catalytic mechanism of SO. The term "exchangeable protons" defines those protons that are readily replaced by deuterons in D_2O solution.

Recently we used pulsed electron paramagnetic resonance (EPR) spectroscopy to investigate the nearby exchangeable protons of the low-pH (lpH) and high-pH (hpH) forms of the Mo(V) center of chicken liver SO in H_2O and D_2O solutions in order to establish their hydroxyl/water coordination structures [5, 6]. Electron spin echo envelope modulation (ESEEM) studies confirmed that the lpH form has a single hydroxyl (Mo-OH) proton lying in the equatorial plane, with a strong isotropic hyperfine interaction (hfi), and which is presumed to be weakly hydrogen-bonded to the S atom of the coordinated cysteine residue (Fig. 1) [6]. The development and application of refocused primary (RP) ESEEM to hpH SO unexpectedly revealed two nearby exchangeable protons in this form [5].

Electron nuclear double resonance (ENDOR) is a complementary technique for directly detecting nearby protons. However, all previous attempts to observe the exchangeable protons of SO by continuous-wave (CW) ENDOR were unsuccessful because of the large linewidths of their ENDOR features (R. LoBrutto et al., Arizona State University, Tempe, AZ, unpubl.). Here we report the first direct detection of the very broad spectrum of the exchangeable proton of lpH SO by pulsed ENDOR, taking advantage of recent improvements in our ENDOR hardware, including a new resonator design and the use of the pulsed mode of the radio-frequency (RF) amplifier. The results for chicken liver SO are com-

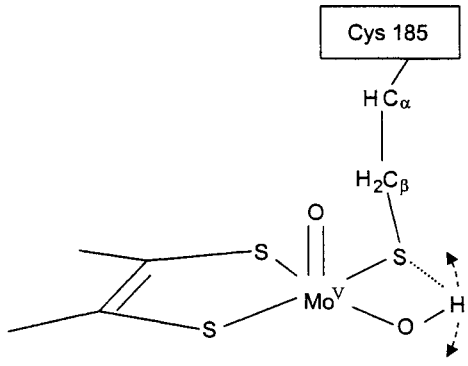

Fig. 1. Structure of the Mo(V) center of lpH SO. The dashed line between the cysteine sulfur ligand and the proton of the OH ligand denotes a suggested weak hydrogen bond. The up and down arrows at the OH ligand hydrogen denote a certain degree of positional disorder for this proton. Most likely, this disorder is associated with a distribution of the OH bond orientations due to restricted rotation of the OH group about the Mo-OH bond.

pared to those for recombinant human SO. We have also used this instrumentation to detect nonexchangeable protons near the Mo(V) active site of SO, in particular, the α-proton of the coordinated cysteinyl residue (Fig. 1), and thereby confirmed that the overall structure of the transient Mo(V) center is similar to that found from X-ray crystallography [7].

2 Experimental

Highly purified chicken liver SO in the lpH form was prepared as previously described [6, 8]. His-tagged recombinant human SO was purified from TP1000 cells containing pTG718 [9]. After harvest, the cells were broken in the presence of a mixture of protease inhibitors supplied as EDTA-free protease inhibitor cocktail tablets (Roche Diagnostics). Chromatography on the NiNTA resin was carried out as described [9] and was followed by a final purification step on DE-52 with a gradient of sodium phosphate buffer, pH 7.8, from 50–350 mM containing 0.1 mM EDTA. The EPR spectrum of the lpH form of His-tagged human SO was obtained in a buffered solution containing 100 mM Tris and 100 mM NaCl. The pH was adjusted to 7.0 by adding 6 M HCl. The protein was reduced anaerobically with a 20-fold excess of sodium sulfite and immediately frozen in liquid nitrogen.

The experiments have been performed on a modified homebuilt X/Ku-band pulsed EPR spectrometer [10] equipped with the cryogenic flow system and a pulsed ENDOR accessory. In the pulsed ENDOR experiments, the Davies technique [11] was employed. The measurement temperature was about 20 K.

3 Results and Discussion

3.1 EPR Spectra

The CW-EPR spectra of lpH SO in H_2O are shown in Fig. 2 (trace 1, chicken SO and trace 4, human SO). The spectra are very similar and show a 7.5 G splitting at the low-field turning point due to the hfi interaction of the hydroxyl ligand (Mo-OH) proton [12]. The splitting of about 11.5 G at the high-field side of the spectra is contributed by both the *g*-anisotropy and the hfi of the hydroxyl (Mo-OH) proton [12]. From the CW-EPR measurements of chicken lpH SO in D_2O the principal *g*-values were determined to be $g_X \approx 1.966$, $g_Y \approx 1.972$ and $g_Z \approx 2.004$ [6, 12] (**X**, **Y** and **Z** are the principal axes of the *g*-tensor, and g_X, g_Y and g_Z correspond, respectively, to g_3, g_2 and g_1 in ref. 12).

The isotropic hfi constant (a_{iso}) and the principal components T_{kk} of the anisotropic hfi tensor of the hydroxyl proton in the chicken lpH SO were determined from the CW-EPR simulations ($a_{iso} = 27.5$ MHz, $T_{11} = -3.7$ MHz, $T_{22} = -5.1$ MHz, $T_{33} = -8.8$ MHz [11]) and from ESEEM measurements ($a_{iso} = 26$ MHz, $T_{11} = T_{22} = -5.12$ MHz, $T_{33} = 10.24$ MHz [6] One can see that the hfi param-

eters obtained by these methods are very similar, although the orientations of the hfi tensor axes **1**, **2** and **3** with respect to the *g*-frame axes were not specified in the CW-EPR work [12]. In the ESEEM work, the main axis (**3**) of the axial hfi tensor was found to be oriented in the XYZ *g*-frame at the polar angle $\theta \approx 82°$ and the azimuthal angle $\varphi \approx 8°$, i.e., virtually along the *g*-tensor axis **X**. The CW-EPR spectrum simulated with the ESEEM parameters (not shown) is in almost perfect agreement with the experimental CW-EPR spectra.

In this work we used a pulsed ENDOR technique to see if there is any significant difference between the hyperfine interactions of Mo(V) with the hydroxyl proton in the chicken and human lpH SO. Performing an ENDOR experiment at different magnetic fields B_0 allows one to selectively observe spectra from the Mo complexes oriented in different ways with respect to the $\mathbf{B}_0$ vector. From such ENDOR spectra the hfi tensor can be determined and its orientation with respect to the *g*-frame can be established.

3.2 ENDOR Spectra

Traces 1, 4 and 7 in Fig. 3 show the Davies ENDOR spectra of chicken lpH SO obtained, respectively, near g_Z, g_Y and g_X. The lines in the range between

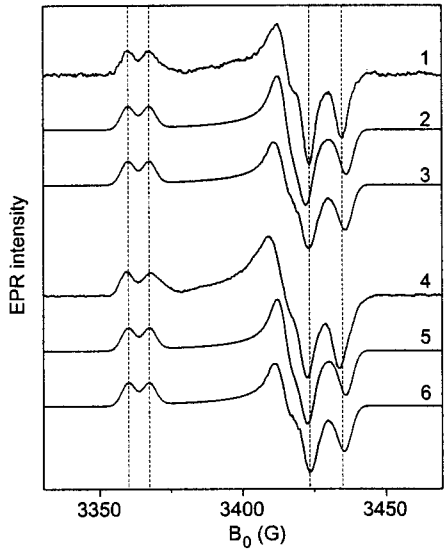

Fig. 2. CW-EPR spectra of chicken (traces 1–3) and human (traces 4–6) lpH SO. Traces 1 and 4, experimental. Experimental conditions: mw frequency, 9.434 GHz; modulation amplitude, 1 G; modulation frequency, 100 kHz; measurement temperature, 77 K. Trace 2, simulated with $a_{iso} = 26.5$ MHz, $T_{11} = -9.2$ MHz, $T_{22} = -7$ MHz, $T_{33} = 16.2$ MHz, $\psi = 90°$, $\theta = 80°$, and $\varphi = 0°$. Trace 5, simulated with $a_{iso} = 26.2$ MHz, $T_{11} = -7.9$ MHz, $T_{22} = -6.7$ MHz, $T_{33} = 14.6$ MHz, $\psi = 90°$, $\theta = 80°$, and $\varphi = 0°$. Traces 3 and 6 are the same as, respectively, traces 2 and 5, but with ψ being uniformly distributed within the limits from 40° to 120°.

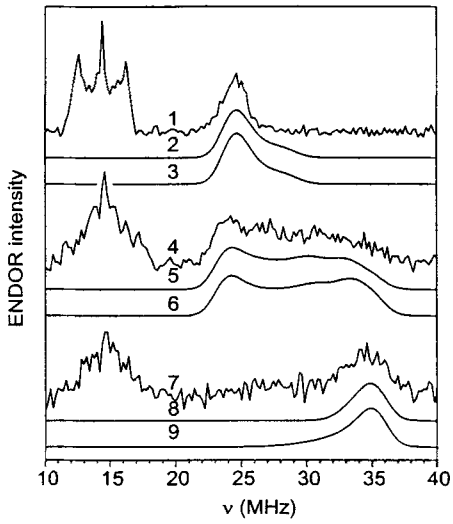

Fig. 3. Davies ENDOR spectra of chicken lpH SO. Traces 1–3, B_0 = 3375 G ($\sim g_Z$). Traces 4–6, B_0 = 3418 G ($\sim g_Y$). Traces 7–9, B_0 = 3439 G ($\sim g_X$). Traces 1, 4 and 7 are the experimental ones. Experimental conditions: mw frequency, 9.446 GHz; mw pulse durations, 40 ns (180°), 20 ns (90°) and 40 ns (180°); time interval between the first and second mw pulses, 40 μs; time interval (τ) between the second and third mw pulses, 400 ns; RF pulse duration, 5 μs; measurement temperature, 20 K. Traces 2, 5 and 8, simulated with a_{iso} = 26.5 MHz, T_{11} = −9.2 MHz, T_{22} = −7 MHz, T_{33} = 16.2 MHz, ψ = 90°, θ = 80°, and φ = 0°. Traces 3, 6 and 9 are the same as, respectively, traces 2, 5 and 8, but with ψ being uniformly distributed within the limits from 40° to 120°.

about 12 and about 17 MHz are mostly due to nonexchangeable protons that have been discussed in a separate work [7]. The strongly coupled hydroxyl proton gives a high-frequency line (ν_β) between 20 and 40 MHz. The low-frequency line (ν_α) was not observed in our X-band experiments because, for this line, a very much longer RF pulse would be required to obtain an optimum ENDOR enhancement factor [13] and a detectable intensity.

Traces 1, 4 and 7 in Fig. 4 show the Davies ENDOR spectra of human lpH SO obtained at g_Z, g_Y and g_X, respectively. One can see that the ENDOR spectra of chicken and human SO are very similar. The similarity of the spectra of the nonexchangeable protons was already noted in our previous work [7]. Here we discuss the spectra of the exchangeable hydroxyl proton.

Davies ENDOR measurements at various B_0 settings have shown that the spectra in Figs. 3 and 4 encompass the whole range of the frequency variation for the hydroxyl proton transition, n_b. Since a_{iso} and T_{33} are of the same sign [6, 12], the fact that the largest hfi constant corresponds to g_X shows that the g-tensor axis **X** is approximately parallel to the main hfi axis **3**, in agreement with the ESEEM results [6]. Accordingly, the spectra at g_Y and g_Z show the line positions corresponding to minimal splittings.

The simulation of the spectra in Figs. 3 and 4 allows one to obtain the hfi parameters for the hydroxyl proton in chicken and human lpH SO. The param-

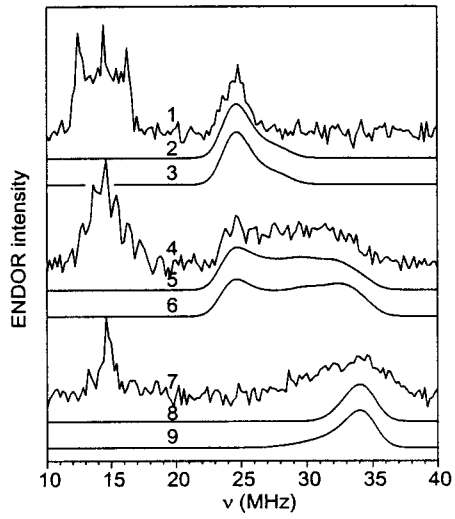

Fig. 4. Davies ENDOR spectra of human lpH SO. Traces 1–3, B_0 = 3375 G ($\sim g_Z$). Traces 4–6, B_0 = 3418 G ($\sim g_Y$). Traces 7–9, B_0 = 3439 G ($\sim g_X$). Traces 1, 4 and 7 are the experimental ones. Experimental conditions: mw frequency, 9.446 GHz; mw pulse durations, 40 ns (180°), 20 ns (90°) and 40 ns (180°); time interval between the first and second mw pulses, 40 μs; time interval (τ) between the second and third mw pulses, 400 ns; RF pulse duration, 5 μs; measurement temperature, 20 K. Traces 2, 5 and 8, simulated with a_{iso} = 26.2 MHz, T_{11} = −7.9 MHz, T_{22} = −6.7 MHz, T_{33} = 14.6 MHz, ψ = 90°, θ = 80°, and φ = 0°. Traces 3, 6 and 9 are the same as, respectively, traces 2, 5 and 8, but with ψ being uniformly distributed within the limits from 40° to 120°.

eters are as follows. In chicken lpH SO, a_{iso} = 26.5 MHz, T_{11} = −9.2 MHz, T_{22} = −7 MHz, T_{33} = 16.2 MHz. The orientation of the hfi frame in the g-frame is given by the Euler angles ψ = 90°, θ = 80° and φ = 0° (ψ, θ and φ are, respectively, the angles of three consecutive rotations: around **3**, around the obtained **1** and around the obtained **3**; with $\psi = \theta = \varphi = 0$ corresponding to the situation of **1** ∥ **X**, **2** ∥ **Y** and **3** ∥ **Z**). For human lpH SO a_{iso} = 26.2 MHz, T_{11} = −7.9 MHz, T_{22} = −6.7 MHz, T_{33} = 14.6 MHz, ψ = 90°, θ = 80°, and φ = 0°. Thus, the parameters for the chicken and human SO are very similar, and their slight difference might simply reflect minor experimental variations in sample preparation.

Comparing the hfi parameters obtained in this work for chicken SO with those obtained by CW-EPR [12] and ESEEM [6] (see above), we find that while all the techniques agree on the isotropic hfi constant of 26–27 MHz, the anisotropic hfi components obtained by ENDOR are, on average, 1.6–1.8 times greater than those obtained by CW-EPR and ESEEM. Correspondingly, the simulation that reproduces the experimental ENDOR spectra (see traces 2, 5 and 8 in Figs. 3 and 4) fails to reproduce the CW-EPR spectra with correct peak positions at the high-field side (see traces 2 and 5 in Fig. 3). For example, the splitting between the high-field turning points of the simulated spectra is noticeably greater than that observed in the experiment, 14.4 G versus 11.5 G. Conversely, the

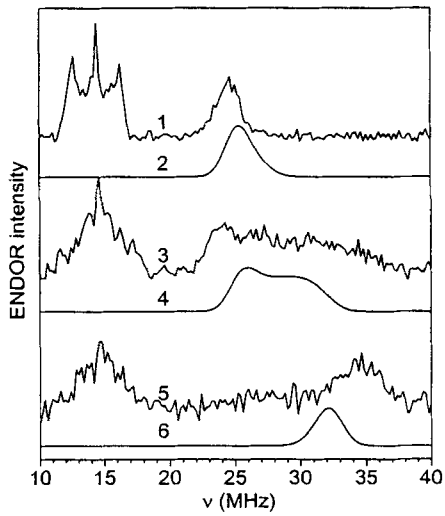

Fig. 5. Davies ENDOR spectra of chicken lpH SO. Traces 1 and 2, $B_0 = 3375$ G ($\sim g_Z$). Traces 3 and 4, $B_0 = 3418$ G ($\sim g_Y$). Traces 5 and 6, $B_0 = 3439$ G ($\sim g_X$). Traces 1, 3 and 5 are the experimental ones, reproduced from Fig. 2. Traces 2, 4 and 6, simulated with $a_{iso} = 26$ MHz, $T_{11} = T_{22} = -5.12$ MHz, $T_{33} = 10.24$ MHz, with the orientation of the main hfi axis (3) in the XYZ g-frame given by the polar angle $\theta \approx 82°$ and the azimuthal angle $\varphi \approx 8°$.

parameters estimated by ESEEM [6] result in a good simulation of the CW-EPR spectrum, but in a very poor simulation of the ENDOR spectra of the chicken lpH SO (see Fig. 5).

The only way to explain the discrepancy between the hfi parameters of the hydroxyl proton obtained by pulsed ENDOR in this work and the previous CW-EPR and ESEEM results is to suggest that the hfi parameters may be statistically distributed within some limits. This distribution may be related to a certain degree of structural disorder in the Mo-OH group (Fig. 1). Thus, the hfi parameters determined by CW-EPR represent average values with all of the variation being included into the individual linewidth (about 5 G). The ESEEM studies [6] were performed on SO in D_2O, and the Mo-OD deuteron spectral line positions were corrupted by the nuclear quadrupole interaction (nqi). In addition, the ESEEM amplitude is zero at the canonical orientations, when $\mathbf{B}_0$ is parallel to the principal axes of the hfi tensor, [14] and this remains approximately true in the presence of weak nqi. Therefore, those studies relied heavily on intensities rather than the positions of the ESEEM spectral lines. With distributed hfi, the observed average intensity has resulted in average hfi parameters close to those determined by CW-EPR.

Unlike ESEEM, ENDOR shows the full extent of nuclear transition lines, including the lines at canonical orientations of $\mathbf{B}_0$. In the ENDOR spectra, the hfi distribution contributes to the line broadening and to the dependence of the line position on the observation point in the CW-EPR spectrum. Generally, with

the hfi distribution involved, the observable CW-EPR splitting will correspond to the center of gravity of the ENDOR line and should not necessarily coincide with the splitting calculated from the ENDOR line maximum.

The properties of the distribution of the hfi values and the related distribution of orientations of the hfi tensor can, in principle, be established from simulations of ENDOR, CW-EPR and ESEEM spectra. However, the detailed implementation of this analysis is extremely time-consuming, and little additional chemical information is expected in this case. Therefore, we restrict ourselves to simulations aimed at qualitatively verifying the trends in the EPR splitting at g_X if the model with a distribution of the hfi parameters is used.

Two types of simulations have been performed. In the first simulation the values of the hfi parameters were fixed, while the orientation of the hfi tensor was varied. It turned out that averaging over the Euler angle ψ uniformly distributed within the limits from 40° to 120° (the average value of 80° is close to $\psi \approx 90°$ found for a fixed hfi tensor) allows one to noticeably reduce the CW-EPR splitting at g_X without significantly affecting the quality of the ENDOR spectra (traces 3 and 6 in Fig. 2, and traces 3, 6 and 9 in Figs. 3 and 4).

In the second simulation, the orientation of the hfi tensor was fixed, while the isotropic and anisotropic hfi values were varied. To ensure the agreement between the experimental and simulated ENDOR spectra at g_Y and g_Z, the principal hfi values $A_{11} = a_{iso} + T_{11}$ and $A_{22} = a_{iso} + T_{22}$ were kept constant (i.e., the variation of a_{iso} was compensated for by the variation of T_{11} and T_{22}). At g_X, on the other hand, the variation of the hfi constant (A_{33}) was maximal, which provided for the average A_{33} value (observed by CW-EPR) being significantly smaller than the maximal A_{33} value (observed by ENDOR). A reasonable fit to the CW-EPR spectrum of the chicken SO (not shown) was obtained for a_{iso}, T_{11}, T_{22} and T_{33} uniformly distributed within the limits [22, 28] MHz, [−4.7, −10.7] MHz, [−2.5, −8.5] MHz and [7.2, 19.2] MHz, respectively (the greater absolute values of a_{iso} correspond to the greater absolute values of T_{kk}). The agreement between the ENDOR spectra was also satisfactory (not shown). For human SO, the "best" distributed values of a_{iso}, T_{11}, T_{22} and T_{33} are within the limits [21.7, 27.7] MHz, [−3.4, −9.4] MHz, [−2.2, −8.2] MHz and [5.6, 17.6] MHz, respectively.

The two limiting descriptions of the distributed hfi parameters discussed above, i.e., structural variations without changes in hfi parameters or hfi parameters that vary in a fixed structure, serve to demonstrate the maximum possible ranges for the variations of structural and hfi parameters. However, these limiting descriptions are clearly simplifications because in reality the changes of the hfi values are caused by changes in the Mo-OH proton location. More precise determination of the parameter distributions would require a model that explicitly relates the structural and hfi parameters. Such a model should be based on extensive quantum chemical calculations and should consider the effects of orientation-dependent spin polarization of the OH oxygen orbitals, including the OH bond orbital, the effects of spin polarization of the sulfur atom of the coordinated cysteine residue, etc. Such a detailed analysis is beyond the scope of this work, although this problem may be addressed in our future publications. Con-

sequently, it is impossible to present a traditional simple estimate for the accuracy of the structural and hfi parameters obtained here, including their distribution widths.

4 Conclusion

In this work we have recorded the pulsed (Davies) ENDOR spectra of the proton of the hydroxyl ligand to the Mo center of the lpH SO. For chicken and human lpH SO, the spectra, and the hfi parameters obtained from them, were very similar. This result is in agreement with our ENDOR study of the nonexchangeable protons and indicates a conservation of structure of the Mo pocket in SO. The hfi parameters determined from the ENDOR spectra were significantly different from those found previously from the CW-EPR and ESEEM spectra. This discrepancy is shown to be related to the fact that the hfi tensor principal values and orientations are statistically distributed. Previously we demonstrated that the positions of nearby protons in the hpH SO, as well as the orientation of the monodentate phosphate ligand in the phosphate-inhibited (*Pi*) form of SO are statistically distributed. In contrast, such a distribution did not follow from the analysis of CW-EPR [12] and ESEEM [6] data for lpH SO. This result was confusing because it suggested a substantial increase in structural order in the vicinity of Mo(V) at pH 7. The data obtained here with pulsed ENDOR show that the coordination of the exchangeable ligand to the Mo(V) site in SO remains disordered at any pH, and the CW-EPR and ESEEM techniques simply were not quite adequate to observe this phenomenon in the case of lpH SO. The positions of the hydroxyl protons in lpH SO and hpH SO, although disordered within certain limits, are still substantially different from one another. In the lpH case, as discussed in ref. 6, the Mo-OH fragment is approximately coplanar with the d_{xy} orbital, which leads to a large isotropic hfi constant for the hydroxyl proton (Fig. 1). In the hpH case, the two nearby exchangeable protons are most probably situated noticeably out of the d_{xy} plane, which leads to practically zero isotropic hfi.

Acknowledgements

We gratefully acknowledge the support of the NIGMS (GM-37773 to J.H.E. and GM44283 to K.V.R.), and we thank the National Science Foundation for funds for construction of the EPR spectrometers (Grants DBI 9604939 and BIR 9224431). We are grateful to Ralph Wiley for assistance in the purification of the recombinant human sulfite oxidase.

References

1. Kisker C., Schindelin H., Pacheco A., Wehbi W.A., Garrett R.M., Rajagopalan K.V., Enemark J.H., Rees D.C.: Cell **91**, 973–983 (1997)

2. George G.N., Pickering I.J., Kisker C.: Inorg. Chem. **38**, 2539–2540 (1999)
3. Rajagopalan K.V. in: Molybdenum and Molybdenum Containing Enzymes (Coughlan M., ed.), pp. 243–272. New York: Pergamon Press 1980.
4. Brody M., Hille R.: Biochemistry **38**, 6668–6677 (1999)
5. Astashkin A.V., Mader M.L., Enemark J.H., Pacheco A., Raitsimring A.M.: J. Am. Chem. Soc. **122**, 5294–5302 (2000)
6. Raitsimring A.M., Pacheco A., Enemark J.H.: J. Am. Chem. Soc. **120**, 11263–11278 (1998)
7. Astashkin A.V., Raitsimring A.M., Feng C., Johnson J.L., Rajagopalan K.V., Enemark J.H.: J. Am. Chem. Soc. **124**, 6109–6118 (2002)
8. Pacheco A., Basu P., Borbat P., Raitsimring A.M., Enemark J.H.: Inorg. Chem. **35**, 7001–7008 (1996)
9. Temple C.A., Graf T.N., Rajagopalan K.V.: Arch. Biochem. Biophys. **383**, 281–287 (2000)
10. Borbat P.P., Raitsimring A.M. in: Abstracts of 36th Rocky Mountain Conference on Analytical Chemistry (Eaton G.R., Eaton S.S., eds.), p. 94. Aurora, CO: Milestones Presentations 1994.
11. Davies E.R.: Phys. Lett. A **47**, 1–10 (1974)
12. Lamy M.T., Gutteridge S., Bray R.C.: Biochem. J. **185**, 397–403 (1980)
13. Grupp A, Mehring M. in: Modern Pulsed and Continuous Wave Electron Spin Resonance (Kevan L., Bowman M., eds.), p. 195. New York: Wiley 1990.
14. Dikanov S.A., Tsvetkov Y.D.: Electron Spin Echo Envelope Modulation, p. 412. Boca Raton: CRC Press 1992.

Authors' address: Arnold M. Raitsimring, Department of Chemistry, University of Arizona, Tucson, Arizona 85721-0041, USA